A DFT Investigation on the Nucleation of Homo- and Heteronuclear Metal Clusters on Defective Graphene

Francesco Ferrante,* Antonio Prestianni, Remedios Cortese, Roberto Schimmenti, and Dario Duca

Dipartimento di Fisica e Chimica - Università degli Studi di Palermo, Viale delle Scienze Ed. 17, 90128 Palermo, Italy

E-mail: francesco.ferrante@unipa.it

Phone: +39 091 23897979. Fax: +39 091 590015

Abstract

Nucleation of homo- (Ni, Pd, Re, Pt) and hetero-metallic (Ni-Pd, Re-Pt) clusters on monovacancy sites of a graphene sheet has been investigated by means of periodic density functional theory calculations. It is shown that a vacant site in graphene is an effective nucleation center both for the monometallic and bimetallic clusters, whose characteristics are described in terms of structural distortions, nucleation energetics, affinities between different metal atoms, metal-carbon interactions and ease of diffusion of metal atoms on graphene.

Introduction

The peculiar interaction between carbon and metal atoms plays a fundamental role in different areas of nanotechnology, such as the preparation of electronic devices[1], catalytic test-

ing,[2–4] and design of new materials.[5–8] Since when it has been isolated as a single sheet of graphite in 2004[9,10], graphene has been the subject of countless studies and has found application in the fields of sensors,[11] biodevices[12] and energy storage.[13] As a matter of fact, it seems that graphene is a suitable material also to be employed as catalytic substrate. Indeed, catalysts prepared from the deposition of metal nanocluster on graphene sheets are nowadays an issue of extreme attractiveness, as regard the occurring of certain catalyzed reactions. Yoo et al.[14] demonstrated that graphene can modify the properties of platinum clusters, which, as a consequence, would reveal a very large activity increase in the methanol oxidation with respect to that of more conventional Pt/carbon-black catalysts. Besides, several catalytic tests showed that also cobalt supported graphene materials have promising catalytic performance in Fischer-Tropsch reaction while a greater stability of graphene has been, in general, observed compared to CNTs.[15]

Reticular defects on graphene can be exploited for the nucleation and growth of small metal clusters. Experimental evidences collected by using scanning transmission electron microscope[16] revealed that it is possible to generate carbon atoms vacancies by means of electron beams. Such vacancies would become trapping sites for metal atoms otherwise free to diffuse on the graphene surface and therefore act as nucleation centers for metal particles.

In the field of supported metal clusters to be used in catalysis, a great relevance is devoted to heteronuclear clusters, whose properties, often, sensibly differ from those of the homonuclear counterparts. Bimetallic particles, indeed, seem to have, in some cases, considerable catalytic activity, selectivity and stability.[17,18] Several structural investigations, along with catalytic activity tests, have been reported for bimetallic supported cluster, characterized by various combinations of Ni, Pd, Re and Pt.[19–21] Further, by means of DFT calculations it has been hypothesized that the occuring of physisorption or chemisorption of H_2 on graphene-supported $Pt_{4-n}Ni_n$ clusters is tightly affected by the composition of the bimetallic particle, suggesting that it is possible to tune the hydrogen adsorption energy, hence the catalytic activity of hydrogenation reactions.[22] Other examples can be found in the recent literature;

e.g., it has been proved that PdPt nanoparticles supported on graphene have a great catalytic activity with respect to the methanol oxidation and the oxygen reduction reactions, showing also an excellent endurance to poisoning,[23] while RePt/γ-Al_2O_3 particles have been successfully employed in the industrial relevant naphtha reforming process.[24]

Finally, metallic or bimetallic clusters nucleated on graphene sheets are interesting also in the field of the hydrogen storage.[25] According to recent studies, transition metal atoms adsorbed on graphene can actually bind one or more hydrogen molecules with interaction energies that have intermediate values between those corresponding to physisorption and chemisorption.[26]

In this work we report a computational investigation dealing with the nucleation of small clusters (up to four atoms) of two common catalytic metals, namely Pd and Pt, as well as of their heteronuclear species formed with Ni or Re, respectively, on a graphene sheet that has a monovacancy defect. This, in order to obtain information on the preferred structures, nucleation geometries and energetics, spin multiplicities and affinities of a given metal atom toward another on the defective graphene.

Models and Computational Details

All the calculations were performed by using the SIESTA method[27] and code, development version 421.[28] The supercell employed for modeling the pristine graphene was comprised of 48 carbon atoms (C_{48}) whereas, as model of the defective graphene, a derived C_{47} system with a carbon vacancy, with respect to the C_{48} one, was considered.

The vdW functional of Dion, Rydberg, Schröder, Langreth and Lundqvist (DRSLL)[29,30] was used and within this framework pseudopotentials and numerical basis sets were generated for C, Ni, Pd, Re and Pt. In particular, relativistic and norm-conserving Troullier-Martins pseudopotentials[31] were generated including non-linear core corrections. Their reliability was tested in a previous work,[32] comparing the atomic orbitals eigenvalues calculated by

them and by an all-electron approach. Furthermore, their transferability was evaluated by calculations *i*) of cohesive energies and bulk moduli (for the metal atoms) and *ii*) of geometrical features of small molecules (for the carbon atom). The strictly confined numerical basis sets peculiar to the SIESTA method were variationally obtained by means of a SIMPLEX algorithm. They are equivalent to double-ζ basis sets plus polarization and to polarization plus diffusion, for the carbon and the metal atoms, respectively.

The C_{48}/C_{47} supercell was replicated in the xy plane, being 1278 pm and 984 pm the lattice constants; 3000 pm was conversely chosen as the z direction lattice constant, in order to simulate the vacuum above the surface. Preliminary tests have been performed in order to develop, within the SIESTA framework, a computational protocol capable to guarantee a satisfactory performance in terms of accuracy and calculation time. It has been found that a $4 \times 4 \times 1$ sampling for the Monkhorst-Pack integration grid and a value of 450 Ry for the mesh cutoff allow to reach a convergence of 0.001 eV for the absolute energy of systems formed by one metal atom inserted on a graphene defect.

In order to simulate the nucleation process in proximity of the defect site the following systematic approach was devised. To start, one metal atom A was placed close to the defect site and the resulting geometry optimized. A second metal atom, either A or B$\neq$A, was thus placed close to A, in turn, in all the possible non-equivalent positions, and the resulting structures were then singly optimized. Starting from the most stable configuration obtained for the A_2/C_{47} and AB/C_{47} systems, a third metal atom, once again A or B, has been added close to the defect. The most stable position for the third atom was, as before, evaluated by geometry optimizations and, in this way, the A_3/C_{47}, A_2B/C_{47} and AB_2/C_{47} systems were generated. Finally, a fourth atom was subjected to the same treatment, following the tree-structure scheme already started. The very same procedure was applied replacing at the first step the B$\neq$A atom in the defect site.

In this way, all the possible configurations of two, three and four metal-atom, both homo- and heteronuclear clusters, were systematically investigated on the graphene defect zone. The

here proposed nucleation algorithm simulates the binding of a metal atom residing on (and moving through) a given graphene surface with another metallic species already trapped in a vacancy defect of the same surface. In addition, the final structure that the clusters adopted close the defective site was also compared with the one adopted by their isolated state counterparts, when calculated at the same level of theory, and in some cases with the corresponding system created by adsorbing on the monovacancy a preformed cluster having the most stable *in vacuo* geometry. The transition states for the diffusion of the metal atoms on pristine graphene, hence the corresponding energy barriers, were evaluated employing the nudged elastic band method,[33,34] by interfacing the SIESTA code to the ASE program.[35]

The following convention will finally be used throughout: when a $M^1M^2 \dots M^n$ symbol is employed to indicate a given cluster, M^1 is the metal atom directly placed on the graphene defect, M^2 is the atom added at the second step and so on up to the M^n, which is the atom introduced as the last.

Definition of nucleation energy

Nucleation energetics is related to the process:

$$\left(M^1 \dots M^{n-1} \; + \; M^n\right)/C_{47} \; \rightarrow \; \left(M^1 \dots M^{n-1}M^n\right)/C_{47}$$

where a M^n metal atom is added to an already existing $M^1 \dots M^{n-1}$ cluster. The system where the adsorbed metal atom and the chemisorbed cluster are, virtually, infinitely far away one from the other was chosen as reference for the nucleation energy, E^n_{nuc}, with $n = 2 - 4$:

$$\begin{aligned} E^n_{nuc} &= E\left[M^1 \dots M^n/C_{47}\right] \\ &- E\left[\left(M^1 \dots M^{n-1} + M^n\right)/C_{47}\right] \end{aligned} \tag{1}$$

In order to calculate the energy term corresponding to the $(\mathrm{M}^1 \ldots \mathrm{M}^{n-1} + \mathrm{M}^n)/\mathrm{C}_{47}$ system, a supercell impossible to treat would have to be used. This problem could be circumvented, assuming the following energy equivalence, stated by adapting an approach already proposed by Schimmenti *et al.*:[36]

$$E_{INT}\left[\mathrm{M}^n/\left(\mathrm{M}^1 \ldots \mathrm{M}^{n-1}/\mathrm{C}_{47}\right)\right] \approx E_{INT}^{CP}\left[\mathrm{M}^n/\mathrm{C}_{48}\right]$$

where $E_{INT}\left[\mathrm{M}^n/\left(\mathrm{M}^1 \ldots \mathrm{M}^{n-1}/\mathrm{C}_{47}\right)\right]$ is the interaction energy occurring between M^n and the graphene surface when the metal atom is far away from the defective zone where the $\mathrm{M}^1 \ldots \mathrm{M}^{n-1}$ cluster is placed; while, $E_{INT}^{CP}\left[\mathrm{M}^n/\mathrm{C}_{48}\right]$ is the interaction energy occurring between a single metal atom and a pristine graphene surface, corrected by using the counterpoise method for the basis set superposition error.[37] As a consequence E_{nuc}^n, could be approximated in terms of absolute energies as:

$$\begin{aligned} E_{nuc}^n &= E\left[\mathrm{M}^1 \ldots \mathrm{M}^n/\mathrm{C}_{47}\right] \\ &- E\left[\mathrm{M}^1 \ldots \mathrm{M}^{n-1}/\mathrm{C}_{47}\right] \\ &- E^{BSSE}\left[\mathrm{M}^n/\mathrm{C}_{48}\right] + E\left[\mathrm{C}_{48}\right] \end{aligned} \tag{2}$$

where $E^{BSSE}\left[\mathrm{M}^n/\mathrm{C}_{48}\right]$ is the energy value of the M^n/C_{48} system, including the BSSE correction, and $E\left[\mathrm{C}_{48}\right]$ the energy term corresponding to the pristine graphene. In order to achieve a relation containing explicit physical insights, Eq. 2 can be rearranged in terms of adsorption energies, ΔE^{ads}, and of the unsupported cluster nucleation energy, $\Delta E_{\mathrm{M}^1 \ldots \mathrm{M}^n}^{nuc,uns}$:

$$\begin{aligned} E_{nuc}^n &= \Delta E_{\mathrm{M}^1 \ldots \mathrm{M}^n/\mathrm{C}_{47}}^{ads} - \Delta E_{\mathrm{M}^1 \ldots \mathrm{M}^{n-1}/\mathrm{C}_{47}}^{ads} \\ &- \Delta E_{\mathrm{M}^n/\mathrm{C}_{48}}^{ads} + \Delta E_{\mathrm{M}^1 \ldots \mathrm{M}^n}^{nuc,uns} \end{aligned} \tag{3}$$

where

$$\Delta E^{nuc,uns}_{\mathrm{M}^1\ldots\mathrm{M}^n} = E_{\mathrm{M}^1\ldots\mathrm{M}^n} - E_{\mathrm{M}^1\ldots\mathrm{M}^{n-1}} - E_{\mathrm{M}^n}$$

Eq. 3 shows that the above defined nucleation energy — besides metal-metal interactions, own of the isolated metallic clusters — involves metal-carbon interactions, related to the adsorption of the metallic species on the defective graphene. It is worth to stress that the terms $\Delta E^{ads}_{\mathrm{M}^1\ldots\mathrm{M}^n/\mathrm{C}_{47}}$ and $\Delta E^{ads}_{\mathrm{M}^1\ldots\mathrm{M}^{n-1}/\mathrm{C}_{47}}$ refer to the adsorption energies of the isolated clusters having the same structure deriving from the nucleation process, which is not necessarily the most stable structure characterizing the corresponding isolated species. Finally, in order to support the interpretation throughout, the cohesive energy of all the homonuclear metallic dimers, trimers and tetramers were calculated at the level of theory used in this work, by employing the relation:

$$E_{coh} = \frac{E_{\mathrm{M}_n} - nE^{CP}_{\mathrm{M}}}{n} \tag{4}$$

where E^{CP}_{M} is the energy of a given metallic atom M corrected for the BSSE by considering as ghost atoms all the other centers in the M_n cluster. The values obtained from Eq. 4 are reported in Table 1.

[Table 1 about here.]

Results and Discussion

Metal/graphene interaction and diffusion

The BSSE-corrected interaction energy values of bare metal atoms with the pristine C_{48} graphene sheet, $E^{CP}_{INT}[M/\mathrm{C}_{48}]$, are collected in Table 2. The rhenium atom shows a very small interaction energy with C_{48}. This is typical of a weak physisorption and is mirrored in the sextet spin multiplicity of the system, which is unchanged with respect to that of the isolated atom. The calculated interaction energy (-0.18 eV) is slightly larger than the

value recently reported by Miramontes *et al.* (−0.136 eV),[38] obtained using an exchange-correlation functional, which did not take into account dispersion interactions. For palladium and platinum, on the other hand, their typical high affinity for carbon is well reproduced, while nickel shows an intermediate value. Among those considered here, nickel is the only metal atom that locates simmetrically at the center of a six-carbon ring and interacts with C_{48} by a η^6 arrangement,[39] with a metal-carbon distance r(Ni-C) value of 224 pm. The Re atom is pretty far from the graphene plane, being 368 pm the smallest r(Re-C) distance value, thus it is not very instructive to describe its interaction geometry. Palladium conversely arranges in the well known[6,40] symmetric η^2 array, with r(Pd-C) equal to 225 pm, while the geometry of the platinum atom is somehow between η^2 and η^1, being r(Pt-C) equal to 216 and 299 pm, respectively.

[Table 2 about here.]

In order to obtain information about the diffusion upon the C_{48} graphene surface, the energy barrier for the displacement of the metal atom from an equilibrium site to another one was calculated. The diffusion of Ni occurs between adjacent rings with a sequence of $\eta^6 - \eta^2 - \eta^6$ arrangements, while that of Pd and Pt occurs between contiguous C−C bonds ($\eta^2 - \eta^1 - \eta^2$). Even for those metal atoms showing a strong interaction with C_{48}, the estimated energy barriers indicate an extremely easy diffusion: 0.09 (Ni), 0.03 (Pd), 0.00 (Re) and 0.09 eV (Pt). These findings are in agreement with the diffusion energy barriers of 4d and 5d metal atoms calculated by Habenicht *et al.*,[41] even if we got a slightly smaller estimate as regards the barrier for platinum. On the whole, the results clearly indicate that the diffusion processes can be neglected in the present investigation while the relocation of one metal atom toward the defect zone, hence the following nucleation and growth, can be considered as a matter of chance. Processes like the diffusion to the defect zone of a cluster formed on a pristine region of the graphene sheet could of course also contribute to clusters formation, as well as nucleation could occur by the approach of polyatomic clusters to a metal seed chemisorbed on the vacancy. However, as discussed by Teng and Sholl,[42] the

mobility of large metal clusters on graphene should be reduced with respect to that of the single atoms. For two- and three-atom species this could be true as well, provided that their adsorption mode does not involve a large number of M-C interactions. For instance, Ni_2, Pd_2 and Pt_2, which adsorb parallel to the graphene surface, would diffuse harder than the corresponding metal atoms, while Ag_2, Re_2 and Au_2, adsorbing perpendicularly, would have almost the same mobility of the atoms. In the present work we assumed that the formation of ultrasmall clusters occurs through a nucleation process involving only species showing very high mobility, i.e. single atoms, considering that the growth by diffusion of polyatomic species should become important in the formation of larger particles.

The optimized geometry of the C_{47} model does not show the 5-9 reconstruction of the defect, typical of graphene with monovacancies.[43–45] This is likely due to the size and to the rectangular shape of the supercell used in the present study. In fact, close to the defect of the C_{47} fragment a clue of 5-5-7 reconstruction is observable, *i.e.* two C−C distances are 234 pm while the one in the short side of the supercell is 259 pm. This can be explained by considering that the small distortions joined with the defect reconstruction propagate in the graphene sheet differently in the long and in the short directions of the supercell. Since the metal atom insertion destroys the reconstruction,[46] this issue should affect only the energetics of the M^1/C_{47} systems and not those regarding the cluster nucleation processes. However, since the lacking of 5-9 reconstruction affects in the same way the interaction energies of all the M^1/C_{47} systems, their relative behaviour is unchanged, so it is worth to report some details about these species, which will be helpful in the discussion that follows.

The geometric parameters characterizing the insertion of one metal atom in the graphene monovacancy are reported in Figure 1. The strong interaction with the metal atom (see Table 2) causes a sensible distortion of the graphene sheet, which can be quantified by the value of a buckling parameter, g_d, representing the height in the z direction of the three carbon atoms to which the metal is bonded (it is zero in the C_{47} system). As it can be noticed, the metal-carbon bond length r(M-C) increases with the atomic number; g_d has the same trend up to Re

but in the Pt system smaller distortions are observed, despite its atomic radius is very similar to that of Re. The calculated binding energies for Ni, Pd and Pt are sensibly smaller than those reported in the literature, evaluated by using the PBE exchange-correlation functional: *ca.* 7 eV for Ni,[46] 5.27 for Pd and 7.23 eV for Pt.[47] With the aim of verifying that the differences between the here binding energy values and those of literature are attributable to the different exchange-correlation functional used, calculations on the M^1/C_{47} systems by employing the PBE functional were performed, leaving all the other settings unchanged. The corresponding pseudopotentials and basis sets were generated and tested with the same procedure used for those employed with the DRSLL functional. The values obtained (Ni: 6.67, Pd: 5.72, Re: 8.03, Pt: 7.09 eV) show that the PBE binding energies are always larger than the DRSLL ones by ca. 0.7 eV, a feature that is, in part, probably due to the extra repulsive term in the revPBE component of the DRSLL parameterization.[29,30] As a matter of fact, this kind of disagreement between PBE and vdW-type functionals was recently pointed out in the literature for metal atoms on graphene[48] and for water adsorption on metal surfaces.[49] To the best of our knowledge, the binding energy of Re with a monovacancy on graphene has never been reported, till now, for comparison.

[Figure 1 about here.]

As regard the magnetic properties of the M^1/C_{47} systems, it has to be taken into account that the calculation gives a spin polarization equal to 1.5 for the defective graphene, in agreement with experimental findings[44] and other computational investigations.[50] Spin coupling would occur when a metal atom is inserted on the defect, with a resulting decreasing of the spin multiplicity in the composite system with respect to that of the isolated atom. In particular, a spin multiplicity lowering of four units was observed for Re (from sextet to doublet) and of two units (from triplet to singlet) for Ni and Pt, while Pd retains its singlet spin state.

Two-atom species

As illustrated in Figure 2, the second metal atom binds to the one already placed on the defect and with it shares the interaction with a carbon atom. This kind of configuration remains unchanged irrespective of the nature of the metal atoms forming the dimers and is common to the first two atoms in trimers and tetramers. In every case, the bond lengthening calculated for the dimer interacting with the defective graphene is less than 10% with respect to the isolated species treated at the same level of calculation. These bond elongations, joined to a spin multiplicity variation, are obviously due to the interaction of the dimers with the defective graphene. All systems containing Ni and/or Pd have singlet spin multiplicity, those containing Pt and Re end-up with a quartet multiplicity when they are in the heteronuclear form, while the singlet state is the most stable when they are in the homonuclear form. It is to note that the isolated homo- and hetero-metallic dimers show ground state spin multiplicities of two units larger than those of the corresponding M^1/C_{47} supercell, thus confirming also in this case an almost perfect spin pairing after the nucleation of the dimer on the graphene defect.

[Figure 2 about here.]

From the data reported in Table 2 it can be stated that, irrespective of the element, the formation of homo- and hetero-metallic dimers on C_{47} is always a largely exoergic process. Since the diffusion of a metal atom on the graphene surface, as already mentioned, is a process requiring the overcoming of very small energy barriers, the formation of metal dimers, hence the nucleation of the metal clusters, should be an easy task. Also, since the reference system is not the M^1/C_{47} species plus an isolated metal atom but the M^1/C_{47} plus a metal atom sited far from the already adsorbed atom on the graphene surface, it is possible to argue that entropic effects are probably not discriminating so that the dimer formation, following the diffusion of a metal atom in direction of the one already sited on the defect, should be also exergonic.

The difference between the nucleation energy of PtRe and all the other dimers involving the same two metals, whose E^2_{nuc} values are essentially identical, can be explained by using Eq. 3 and the values reported in Table 2. In fact, it must be considered that according to our calculations the $\Delta E^{nuc,uns}$ contribution is almost the same for all the dimers in the Re-Pt class (ca. -3.3 eV). These values obviously correspond to an estimate of the binding energies of the molecules, which in the Re_2 and Pt_2 cases have experimental counterparts of 4 ± 1 and 3.14 eV, respectively.[51] On the other hand, the adsorption energy $\Delta E^{ads}_{M^1M^2/C_{47}}$ is -6.4, -7.3 and -6.3 eV for ReRe, RePt and PtPt, respectively, but is only -4.4 eV for PtRe. The nucleation energy values for the Re-Pt dimers are therefore the result of the opposite trends shown by Re and Pt with respect to the magnitude of the metal-defect and metal-carbon interactions.

Three-atom species

When a third atom approaches and binds to the dimer located on the graphene defect zone, two main arrangements could occur: a trimer whose atoms all interact with the graphene surface or one where the third metal atom interacts only with the already adsorbed dimer. The balance between metal-graphene and metal-metal interactions rules the occurrence of the arrangement that actually takes place. It can be indeed argued that if the metal-graphene interactions were predominant the triatomic cluster would adopt a distorted triangular structure oriented, some way, parallel to the graphene plane. If instead the metal-metal were stronger than the metal-graphene interactions, two different cases should be considered: in the first, it is possible to postulate that the cluster structure and the nucleation geometry are such to equally admit both kinds of interactions. In this case, the supported cluster should have a shape similar to that of the corresponding isolated species and furthermore, would interact well with the defect without any, or very small, structural changes. In the second, it can be hypothesized that in order to efficiently interact with the defective site, large distortions of the cluster structure should occur but, since the metal-metal interactions are

stronger, the cluster lies on the plane in such a way that only some of its atoms interact with graphene. In order to give a qualitative description of the triatomic cluster rearrangements, a simple distortion parameter, λ, can be introduced:

$$\lambda = \frac{1}{n} \sum_{i=1}^{n} \left(\frac{l_i}{l_0} \right) \tag{5}$$

where n is the number of bonds characterizing the considered cluster (*e.g.* $n = 3$ for the trimeric species), l_i is conversely a given M−M bond length of the cluster interacting with graphene while l_0 is the corresponding bond length in the isolated species. Since all the considered isolated triatomic clusters have a triangular structure, the value of the λ parameter reflects also the angular distortions. If the trimer nucleation energy, E^3_{nuc}, is reported against λ, the graphs of Figure 3 are obtained.

[Figure 3 about here.]

It can be noticed that the clusters containing Ni and Pd have λ values spanning a narrow range comprised between 1.01 and 1.08. All the λ values are greater than 1, which means that the M−M bond lengths are, in the average, longer than those of the corresponding isolated species. Each cluster, belonging to the trimer set, shows a nucleation geometry for which the metal trimer lies on the graphene surface; the only exception is NiNiPd, to which the smallest value of λ is associated. It is possible to notice that all the clusters with a larger content of Ni show λ values closer to 1 than those with larger content of Pd, provided that the atom directly placed on the defect is not the outnumbered one. This could be related to the higher energetic content of the Ni−Ni with respect to the Pd−Pd bond that, inter alia, can be easily inferred considering the cohesive energy values reported in Table 1, which are in line with the experimental bulk cohesive energy of the two metals (*i.e.* 4.44 and 3.89 eV/atom for Ni and Pd, respectively). The overall effect could be summarized stating that increasing the Ni content in the trimer the metal-metal interactions rise, leading to less distorted clusters on the graphene defect.

Trimers containing Re and Pt have λ values ranging from 0.92 to 1.04, except for the PtPtPt cluster, which shows the highest λ value (1.17) in the series. Some Re-Pt clusters have λ smaller than — or very close to — the unity, revealing minute distortions. In details, RePtPt, PtPtRe and PtRePt are those clusters showing $\lambda < 1$; their reference cluster in the isolated state is the angular PtRePt, having quartet multiplicity and two Pt atoms each other (Pt−Pt distance of 441 pm) not bonded. In the Pt-Re clusters above, conversely, the two Pt atoms are bonded due to favourable interactions that occur with the defect zone of graphene: the resulting Pt−Pt distances are 265, 268 and 273 pm, respectively. The net result is a nucleation energy sensibly smaller than that of the other clusters in the Re-Pt set where the Re−Re bond can be found. It is to be noticed that all the Re-Pt trimers are almost perpendicular to the graphene sheet, with one of the vertex interacting with the defect and one bonded to a carbon atom. Comparing the E^3_{nuc} *vs.* λ trends for the Ni-Pd and Re-Pt cluster sets, two main interesting features appear (see Figure 3): *i*) the different spread of the λ values and *ii*) the trimer interaction geometry that, in the Ni-Pd case, is characterized by a parallel arrangement of the metal trimer with respect to the graphene surface while in the Re-Pt case by a perpendicular one. It is possible to infer that both the features above are very likely due to a predominant metal-metal component present in the Re-Pt trimers, which is even higher than in the Ni-Pd case. With respect to this, it should be noticed that both Pt and Re actually show higher bulk cohesive energies with respect to Ni and Pd (8.03 and 5.84 eV/atom for Re and Pt, respectively). A representative selection of three- and four-atom cluster geometry on C_{47} is reported in Figure 4.

[Figure 4 about here.]

The nucleation energies of the Ni-Pd trimers are comprised between −1.25 and −1.95 eV. In this cluster set, it seems that there are not sensible differences in the nucleation energetics when a third atom is bound to a given dimer already placed on the defective graphene. An inspection to Figure 5, where the nucleation energy values are reported for the three-atom, E^3_{nuc}, and four-atom, E^4_{nuc}, clusters, allow us to conclude that the largest

difference in the nucleation energy is 0.33 eV, being the NiPdNi cluster more stable than the NiPdPd one. The smallest E^3_{nuc} value is conversely 0.03 eV, *i.e.* the NiNi dimer, whose formation on the defective graphene is preferred to that of NiPd (see Table 2), generates the NiNiNi or the NiNiPd cluster almost involving the same energy. This low "discriminating power" could be linked to the relatively low difference in cohesive energies of these two metals (0.55 eV/atom) and to the scarce difference between their affinities to the pristine graphene ($E^{CP}_{INT}[Ni/\mathrm{C}_{48}] - E^{CP}_{INT}[Pd/\mathrm{C}_{48}] = 0.30$ eV, see Table 2). Qualitatively, the increase of Ni content is related to trimer formation showing more negative nucleation energy. The relative stability of the trimers shares the same trend of their two-atoms nucleation seeds (NiNi > NiPd > PdNi > PdPd), with those increasing the Ni content always favoured with respect to those involving a new Pd atom.

Letting aside the PtPtPt cluster, which has the relatively low nucleation energy of -1.27 eV, the remaining Re-Pt trimers are characterized by a nucleation energetics much larger than that associated to the Ni-Pd clusters. It indeed ranges from -2.28 eV (PtPtRe) to the very high value of -5.01 eV (ReReRe). These values are clearly in agreement with the larger bulk cohesive energies of the Pt and Re with respect to Ni and Pd. On the whole, the higher E^3_{nuc} values of the Re-Pt cluster set, but the PtPtPt species, are also related to the low affinity of the rhenium atom toward graphene, which affects, as suggested by Eq. 3, the nucleation energies. In fact, the clusters with low Re content, and in particular PtPtPt, have smaller nucleation energy values, showing the Pt atom a good affinity for graphene. To end, the dimeric species in the Re-Pt class should be able to discriminate the features of the third incoming metal atom: now the smallest difference between the growth energy of a dimer with respect to the third atom is 0.61 eV (PtRe) and is *ca.* 1 eV for all the other dimeric species. In any case, the dimers of the Re-Pt cluster set are more prone to react with Re rather than with Pt to give a trimer. The discriminating power in ruling the nucleation of a third metallic atom is clearly larger for the Re-Pt than for the Ni-Pd set. However, as for the latter, the discriminating power of the Re-Pt set is mainly related to the metal

cohesive energy difference, very pronounced in this case (*i.e.* 2.19 eV/atom).

[Figure 5 about here.]

Four-atom species

In Figure 6, the E^4_{nuc} values corresponding to all the clusters of both the Ni-Pd and Re-Pt sets are reported *versus* the matching λ values, calculated by Eq. 5, setting $n = 6$. As reference for the evaluation of the distortions of a given metal species nucleating on graphene, the structure of the isolated cluster having the most similar geometry to that of the chemisorbed cluster was chosen. It is important to notice that for all the Ni-Pd set members, irrespective of the starting cluster configuration and geometry, the optimization of the isolated fragments invariably converges into a tetrahedral species (See Figure 4). Therefore, just five types of isolated clusters have been used as references for the Ni-Pd species, namely the two homo-metallic and the three hetero-metallic ($NiPd_3$, Ni_2Pd_2 and Ni_3Pd) tetrahedral structures. On the other hand, when the Re-Pt clusters are considered, a structure very similar to that of the adsorbed one, almost always, exists also in the isolated state.

[Figure 6 about here.]

The metal clusters in the Ni-Pd class have λ values in-between 0.99 and 1.18; two regions in the corresponding graph can be identified: in the first are included those points placed below $\lambda = 1.05$. These are associated to clusters showing tetrahedral structure. In the second — above that value of λ —, are conversely included those points corresponding to metal clusters adopting a butterfly geometry, *i.e.* a tetrahedron-like non-planar structure with a broken side (two kinds of butterfly arrangements are showed in Figure 4). Here, it is worth describing the case of the Ni_4 and Pd_4 clusters, since they were the subject of analogous investigations already reported in the literature. The structure of Ni_4 was actually studied both as isolated species and adsorbed on pristine graphene.[52] According to that investigation, the isolated Ni_4 is in a quintet spin state and resembles a symmetrically

distorted tetrahedron, with four Ni−Ni distances longer than the other two. The most stable structure of the Ni_4 cluster, when adsorbed on the surface of a pristine graphene sheet, is a perfect tetrahedron with triplet multiplicity. The here calculations give the same spin multiplicity for the isolated Ni_4 while when chemisorbed on C_{47}, it is in a singlet state. Slightly longer Ni−Ni distances are observed in the first case, whereas expected — although small ($\lambda = 1.01$) — asymmetric distortions characterize the second, where the tetrahedron lies with a vertex on the defect and another bonded to a carbon atom.

A different arrangement marks the Pd_4 clusters. According to the present calculations and to the literature data,[53] the isolated Pd_4 cluster has a slightly distorted tetrahedral geometry. Furthermore, following Ramos-Castillo *et al.*[54] when Pd_4 is placed on a graphene monovacancy it should maintain its tetrahedral structure. The present calculation would conversely suggest a butterfly geometry, generating a large value of the distortion parameter ($\lambda = 1.18$) and a small nucleation energy value ($E^4_{nuc} = -1.41$ eV). As a matter of fact, if a tetrahedral Pd_4 fragment is optimized on the defect without considering the nucleation algorithm thoroughly employed in this work, a minimum is obtained, which is 0.55 eV more stable than the butterfly one, being $\lambda = 1.01$. Therefore, it is possible to hypothesize that the butterfly geometry — corresponding to a local minimum when Pd_4 is anchored on the defect— is consequent to the nucleation process, which therefore can give cluster structures dissimilar from those obtained from the mere chemisorption on the graphene defect of a preformed cluster. Further, the different behaviour of Ni_4 and Pd_4 with respect to the geometry adopted, following the nucleation (the former converting to a tetrahedron, the latter not) could be correlated to the fact that the Ni−Ni bond is stronger than the Pd−Pd while the Ni−C interaction is weaker than Pd−C.

All of the Re-Pt clusters in the M^4/C_{47} systems have λ values in the range $0.98 - 1.10$. In the low end of this interval there is one point, corresponding to the highly distorted tetrahedral PtReReRe species. The remaining Re-Pt clusters have butterfly-like geometries. In details, those clusters with λ very close to 1 consist of butterfly structures, interacting almost

perpendicularly with the graphene sheet and having just one atom placed in correspondence of the defective site. Conversely, the point at $\lambda = 1.10$ is associated to the RePtReRe cluster that, when isolated, has a butterfly structure with a Re−Re bond easily recognizable, while, when chemisorbed, a structure distorted by the breaking of the Re−Re bond and the formation of a new Re−Pt bond, which gives rise to the higher value of λ.

The behaviour of the Re_4 and Pt_4 clusters on the defect is somehow similar to that of the Ni_4 and Pd_4 cases. In particular, the Re_4 species has a tetrahedral structure either when isolated or nucleated on the vacancy defect and, while the Re−Re bond is very strong, the Re−C interaction seems to be extremely weak. To our knowledge, the investigation of the properties of this cluster on a graphene monovacancy was, up to now, never performed. The case of Pt_4, on the other hand, is rather enlightening: in fact, even if Pt has a bulk cohesive energy larger than that of Ni, it behaves like the Pd_4 cluster. It adopts a butterfly structure when nucleated in the defect zone while the preformed tetrahedral cluster, when chemisorbed on the defect, is more stable (0.30 eV) and suffers only slight structural distortions ($\lambda = 1.02$) whit respect to the isolated counterpart. This evidence can be explained taking into account that the Pt−C interaction seems to be the largest among those of the here investigated metals and, effectively, a Pt_4 cluster with butterfly geometry is a minimum even in the isolated state, differing only 0.12 eV in energy from the most stable tetrahedral geometry. As a matter of fact, the existence of a butterfly Pt_4 cluster interacting with a monovacancy on graphene was already reported,[55] though, it was not discussed from the nucleation point of view. Also in this case, therefore, the nucleation process would give a cluster geometry corresponding to a local minimum as a result of M−C interactions.

On the whole, the Re-Pt tetratomic clusters show larger nucleation energies than the Ni-Pd ones, even if the differences are now reduced with respect to those calculated for the triatomic species. This could be tentatively rationalized in terms of the analysis reported above. Generally speaking, the Ni-Pd four-atom clusters with values of λ close to 1 do not show very efficient interactions with graphene, while those with higher values of λ do. This

because large geometry distortions, which decrease the occurrence of metal-metal interactions, are to be ascribed to strong M-C interactions. The Re-Pt clusters are, on the contrary, less sensible to the local atom arrangement in their structure: indeed, it seems that they can interact efficiently with graphene and, at the same time, maintain good interactions between the metal centers or, from an opposite point of view, they can sit on the defect without relevant distortions of the isolated butterfly geometry. Further, in most of the clusters showing E^4_{nuc} larger than -3 eV, Re is the fourth nucleating atom, so that the nucleation energy could be affected by the low affinity of Re toward C, as discussed for the three-atom species.

By referring to Figure 5, the nucleation energies associated to the four-atom clusters formation inside the two classes of metallic species is now discussed. The largest nucleation energies are shown by NiNiNiNi and NiNiPdNi (-2.68 and -2.88 eV); the smallest by the NiPdNiPd and NiPdPdPd clusters (-1.37 and -1.39 eV). On the other hand, when Pd is the first atom, the nucleation energy of the four-atom cluster is always larger than that of the three-atom counterpart, reaching the maximum value (-3.21 eV) for the PdNiNiNi case. A very low nucleation energy (-1.41 eV) is associated to the PdPdPdPd cluster. These findings are in agreement with the evidences pointed out along with the trimer analysis that stated a connection between the increase of the nucleation energy, E^3_{nuc}, and the Ni content. The PdPdNi and PdPdPd three-atom species, actually, seem to not be able to discriminate between Ni or Pd as the fourth nucleating atom. On the other hand, three of the four trimers, having a Ni atom placed in the defect site, invariably favour binding of a fourth Ni atom: NiNiNiNi is, indeed, more stable than NiNiNiPd by 1.15 eV, NiPdNiNi than NiPdNiPd by 1.51 eV and NiPdPdNi than NiPdPdPd by 1.04 eV; the affinity of Pd toward graphene could clearly contribute to this issue. For all the remaining Ni-Pd systems, the difference between the two possible E^4_{nuc} values is around 0.5 eV.

In the majority of cases, E^3_{nuc} is larger than E^4_{nuc} in the Re-Pt cluster set. Important exceptions are all the four clusters, which start their nucleation from the PtPt dimer and, to a minor extent, the RePtPtRe cluster. By passing from PtPtRe to PtPtReRe there is an

energy gain of 3.69 eV and, noticeably, the PtPtPtPt cluster, whose corresponding trimer is characterized by $E^3_{nuc} = -1.27$ eV, has $E^4_{nuc} = -2.70$ eV. The discriminating power toward nucleation of a fourth metal atom of the Re-Pt three-atom clusters is similar to that already shown by the two-atom species. In details, the most discriminating are ReReRe, PtPtRe and RePtPt, which favour the binding of Re with respect to Pt by 1.01, 1.26 and 0.90 eV while, all the other trimers are characterized by values close to 0.6 eV (mostly, favouring the Re entrance). The RePtRe species is an exception, being associated to a value equal to 0.3 eV. Once again, the different affinity of Pt and Re toward graphene, joined with the inter-metallic cohesive energy differences — characterizing the metals involved in the cluster formation — should contribute to the discriminating behaviour above described.

Conclusions

Periodic DFT calculations within the SIESTA formalism were performed, in order to investigate the formation of homo- and hetero-metallic Ni-Pd and Re-Pt clusters — formed by, up to, four metallic atoms — on a defect of a graphene model, having one vacant site. The results were discussed in terms of cluster structure variations, metal-metal as well as metal-carbon affinities and nucleation energies. The latter was defined as a function of a bond distortion parameter related to *i*) the metal bulk cohesive energies, *ii*) the magnitude of the metal-carbon interactions, which take place either on the defective or on the pristine graphene surface, and *iii*) the relative stability of the nucleation seeds. As a general trend, small bulk cohesive energies give rise to distorted structures of the supported cluster and small nucleation energies, which also decreases with increasing the affinity of the involved metal atoms toward the defect-free graphene. The difference in the bulk cohesive energy of the considered metals surely affects the discriminating power in ruling the nucleation of a new metal atom on an already formed metallic cluster. The differences in the bulk cohesive energies, however, begin to be substantially relevant for the largest clusters, namely for the

four-atom species. In these, a high Ni (Re) content leads preferably to the binding of new Ni (Re) atoms, suggesting that, possibly after structural rearrangements, small particles with Ni (Re) cores and Pd (Pt) shells could be preferentially formed. The analysis of the structural characteristics, furthermore, suggests that when the metal-metal interactions prevail on the metal-carbon ones, the nucleated cluster adopts, after some distortions, the same geometry shown in the isolated state, leading to a surface species not very different with respect of that obtained following the chemisorption of a preformed clusters. Conversely, if metal-metal and metal-carbon interactions have comparable intensity, nucleation usually brings to cluster geometries that could correspond to metastable (or even unstable) structures in the isolated state. This behaviour can clearly affect growth, hence shape, of large metal clusters on graphene. Finally, since the graphene defective sites are powerful nucleating centers, a graphene sheet having many vacant sites should permit the generation of a large number of small metal clusters. This is certainly a desirable feature to be exploited both in catalysis and hydrogen storage technology. In particular, the metal cluster anchoring on the graphene defects could block the competitive desorption of H_2 and of the cluster itself, which represent a well known crucial problem of the hydrogen storage processes.

Acknowledgement

Funding is gratefully acknowledged by European Union Seventh Framework Programme (FP7/2007- 2013) within the project SusFuelCat: "Sustainable fuel production by aqueous phase reforming – understanding catalysis and hydrothermal stability of carbon supported noble metals" GA: CP-IP 310490 (http://cordis.europa.eu/projects/rcn/106702_en.html).

References

(1) Banhart, F. Interactions between Metals and Carbon Nanotubes: at the Interface between Old and New Materials. *Nanoscale* **2009**, *1*, 201–2013.

(2) D'Anna, V.; Duca, D.; Ferrante, F.; La Manna, G. DFT Studies on Catalytic Properties of Isolated and Carbon Nanotube Supported Pd_9 Cluster-I: Adsorption, Fragmentation and Diffusion of Hydrogen. *Phys. Chem. Chem. Phys.* **2009**, *11*, 4077–4083.

(3) Ferrante, F.; Prestianni, A.; Duca, D. Computational Investigation of Alkynols and Alkyndiols Hydrogenation on a Palladium Cluster. *J. Phys. Chem. C* **2014**, *118*, 551–558.

(4) Crespo-Quesada, M.; Yoon, S.; Jin, M.; Prestianni, A.; Cortese, R.; Cárdenas-Lizana, F.; Duca, D.; Weidenkaff, A.; Kiwi-Minsker, L. Shape-Dependence of Pd Nanocrystal Carburization during Acetylene Hydrogenation. *J. Phys. Chem. C* **2015**, *119*, 1101–1107.

(5) Machado, B. F.; Serp, P. Graphene-based materials for catalysis. *Catal. Sci. Technol.* **2012**, *2*, 54–75.

(6) Prestianni, A.; Ferrante, F.; Sulman, E. M.; Duca, D. Density Functional Theory Investigation on the Nucleation and Growth of Small Palladium Clusters on a Hyper-Cross-Linked Polystyrene Matrix. *J. Phys. Chem. C* **2014**, *118*, 21006–21013.

(7) Hu, J.; Zhu, Z.; Wu, R. Chern Half Metals: A New Class of Topological Materials to Realize the Quantum Anomalous Hall Effect. *Nano Letters* **2015**, *15*, 2074–2078.

(8) Kumar, R.; Oh, J.-H.; Kim, H.-J.; Jung, J.-H.; Jung, C.-H.; Hong, W. G.; Kim, H.-J.; Park, J.-Y.; Oh, I.-K. Nanohole-Structured and Palladium-Embedded 3D Porous Graphene for Ultrahigh Hydrogen Storage and CO Oxidation Multifunctionalities. *ACS Nano* **2015**, *9*, 7343–7351.

(9) Novoselov, K. S.; Geim, A. K.; Morozov, S. V.; Jiang, D.; Zhang, Y.; Dubonos, S. V.; Grigorieva, I. V.; Firsov, A. A. Electric Field Effect in Atomically Thin Carbon Films. *Science* **2004**, *306*, 666–669.

(10) Geim, A. K.; Novoselov, K. S. The Rise of Graphene. *Nat. Mater.* **2007**, *6*, 183–191.

(11) Castro-Neto, A. H.; Peres, N. M. R.; Novoselov, K. S.; Geim, A. K. The Electronic Properties of Graphene. *Rev. Mod. Phys.* **2009**, *81-162*, 109.

(12) Geim, A. K. Graphene: Status and Prospects. *Science* **2009**, *324*, 1530–1534.

(13) Raccichini, R.; Varzi, A.; Passerini, S.; Scrosati, B. The Role of Graphene for Electrochemical Energy Storage. *Nat. Mater.* **2015**, *14*, 271–279.

(14) Yoo, E.; Okata, T.; Akita, T.; Kohyama, M.; Nakamur, J.; Honma, I. Enhanced Electrocatalytic Activity of Pt Subnanoclusters on Graphene Nanosheet Surface. *Nano Lett.* **2009**, *9*, 2255–2259.

(15) Karimi, S.; Tavasoli, A.; Mortazavi, Y.; Karimi, A. Cobalt Supported on Graphene – A Promising Novel Fischer–Tropsch Synthesis Catalyst. *Appl. Catal. A: Gen.* **2015**, *499*, 188–196.

(16) Rodríguez-Manzo, J. A.; Cretu, O.; Banhart, F. Trapping of Metal Atoms in Vacancies of Carbon Nanotubes and Graphene. *ACS Nano* **2010**, *4*, 3422–3428.

(17) Wen, D.; Guo, S.; Wang, Y.; Dong, S. Bifunctional Nanocatalyst of Bimetallic Nanoparticle/TiO2 with Enhanced Performance in Electrochemical and Photoelectrochemical Applications. *Langmuir* **2010**, *26*, 11401–11406.

(18) Peng, Z.; Yang, H. Synthesis and Oxygen Reduction Electrocatalytic Property of Pt-on-Pd Bimetallic Heteronanostructures. *J. Am. Chem. Soc.* **2009**, *131*, 7542–7543.

(19) Koh, A. C. W.; Chen, L.; Leong, W. K.; Ang, T. P.; Johnson, B. F. G.; Khimyak, T.; Lin, J. Ethanol Steam Reforming over Supported Ruthenium and Ruthenium–Platinum Catalysts: Comparison of Organometallic Clusters and Inorganic Salts as Catalyst Precursors. *Int. J. Hydrogen Energ.* **2009**, *34*, 5691–5703.

(20) Meitzner, G.; Via, G. H.; Lytle, F. W.; Sinfelt, J. H. Structure of Bimetallic Clusters. Extended X-Ray Absorption Fine Structure (EXAFS) of Pt-Re and Pd-Re Clusters. *J. Chem. Phys.* **1987**, *87*, 6354–6363.

(21) Fung, A. S.; Kelley, M. J.; Koningsberger, D. C.; Gates, B. C. γ-Al2O3-Supported RePt Cluster Catalyst Prepared from $[Re_2Pt(CO)_{12}]$: Characterization by Extended X-ray Absorption Fine Structure Spectroscopy and Catalysis of Methylcyclohexane Dehydrogenation. *J. Am. Chem. Soc.* **1997**, *119*, 5877–5887.

(22) Wu, J.; Ong, S. W.; Kang, H. C.; Tok, E. S. Hydrogen Adsorption on Mixed Platinum and Nickel Nanoclusters: The Influence of Cluster Composition and Graphene Support. *J. Phys. Chem. C* **2010**, *114*, 21252–21261.

(23) Khan, M.; Yousaf, A. B.; Chen, M.; Wei, C.; Wu, X.; Huang, N.; Qi, Z.; Li, L. Mixed-Phase Pd-Pt Bimetallic Alloy on Graphene Oxide with High Activity for Electrocatalytic Applications. *J. Power Sources* **2015**, *282*, 520–528.

(24) Kluksdahl, H. Reforming a Sulfur-Free Naphtha with a Platinum-Rhenium Catalyst. 1968; US Patent 3,415,737.

(25) Sen, D.; Thapa, R.; Chattopadhyay, K. K. Small Pd Cluster Adsorbed Double Vacancy Defect Graphene Sheet for Hydrogen Storage: A First-Principles Study. *Int. J. Hydrog. Energy* **2013**, *38*, 3041–3049.

(26) Cabria, I.; López, M. J.; Fraile, S.; Alonso, J. A. Adsorption and Dissociation of Molecular Hydrogen on Palladium Clusters Supported on Graphene. *J. Phys. Chem. C* **2012**, *116*, 21179–21189.

(27) Soler, J. M.; Artacho, E. J.; Gale, D.; García, A.; Junquera, J.; Ordejón, P.; Sánchez-Portal, D. The SIESTA Method for Ab-Initio Order-N Materials Simulation. *J. Phys.: Cond. Matt.* **2002**, *14*, 2745–2779.

(28) Sánchez-Portal, D.; Ordejón, P.; Artacho, E. J.; Soler, J. M. Density Functional Method for Very Large Systems with LCAO Basis Sets. *Int. J. Quant. Chem.* **1997**, *65*, 453–461.

(29) Langreth, D. C.; Dion, M.; Rydberg, H.; Schröder, E.; Hyldgaard, P.; Lundqvist, B. I. Van der Waals Density Functional Theory with Applications. *Int. J. Quant. Chem.* **2004**, *101*, 599–610.

(30) Dion, M.; Rydberg, H.; Schröder, E.; Langreth, D. C.; Lundqvist, B. I. Van der Waals Density Functional for General Geometries. *Phys. Rev. Lett.* **2004**, *92*, 246401.

(31) Troullier, N.; Martins, J. L. Efficient Pseudopotentials for Plane-Wave Calculations. *Phys. Rev. B* **1991**, *43*, 1993–2006.

(32) Cortese, R.; Schimmenti, R.; Armata, N.; Ferrante, F.; Prestianni, A.; Duca, D.; Murzin, D.-Y. Investigation of Polyol Adsorption on Ru, Pd, and Re Using vdW Density Functionals. *J. Phys. Chem. C* **2015**, *119*, 17182–17192.

(33) Mills, G.; Jónsson, H. Quantum and Thermal Effects in H_2 Dissociative Adsorption: Evaluation of Free Energy Barriers in Multidimensional Quantum Systems. *Phys. Rev. Lett.* **1994**, *72*, 1124–1127.

(34) Villarba, M.; Jónsson, H. Diffusion Mechanisms Relevant to Metal Crystal Growth: Pt/Pt(111). *Surf. Sci.* **1994**, *317*, 15–36.

(35) Bahn, S. R.; Jacobsen, K. W. An Object-Oriented Scripting Interface to a Legacy Electronic Structure Code. *Comput. Sci. Eng.* **2002**, *4*, 56–66.

(36) Schimmenti, R.; Cortese, R.; Ferrante, F.; Prestianni, A.; Duca, D. Growth of Sub-Nanometric Palladium Clusters on Boron Nitride Nanotubes: a DFT Study. *Phys. Chem. Chem. Phys.* **2016**, *118*, 1750–1757.

(37) Boys, S.; Bernardi, F. The Calculation of Small Molecular Interactions by the Differences of Separate Total Energies. Some Procedures with Reduced Errors. *Mol. Phys.* **1970**, *19*, 553–566.

(38) Miramontes, O.; Bonafé, F.; Santiago, U.; Larios-Rodriguez, E.; Velázquez-Salazar, J. J.; Mariscal, M. M.; Yacaman, M. J. Ultra-Small Rhenium Clusters Supported on Graphene. *Phys. Chem. Chem. Phys.* **2015**, *17*, 7898–7906.

(39) Eelbo, T. et al. Adatoms and Clusters of 3d Transition Metals on Graphene: Electronic and Magnetic Configurations. *Phys. Rev. Lett.* **2013**, *110*, 136804.

(40) Granatier, J.; Lazar, P.; Otyepka, M.; Hobza, P. The Nature of the Binding of Au, Ag, and Pd to Benzene, Coronene, and Graphene: From Benchmark CCSD(T) Calculations to Plane-Wave DFT Calculations. *J. Chem. Theory Comput.* **2011**, *7*, 3743–3755.

(41) Habenicht, B. F.; Teng, D.; Semidey-Flecha, L.; Sholl, D. S.; Xu, Y. Adsorption and Diffusion of 4d and 5d Transition Metal Adatoms on Graphene/Ru(0001) and the Implications for Cluster Nucleation. *Top. Catal.* **2014**, *57*, 69–79.

(42) Teng, D.; Sholl, D. S. Adsorption and Diffusion of Rh and Au Dimers and Trimers on Graphene/Ru(0001). *Surf. Sci.* **2014**, *626*, 6–13.

(43) Cretu, O.; Krasheninnikov, A. V.; Rodrìguez-Manzo, J. A.; Sun, L.; Nieminen, R. M.; Banhart, F. Migration and Localization of Metal Atoms on Strained Graphene. *Phys. Rev. Lett.* **2010**, *105*, 196102.

(44) Chen, J.-J.; Wu, H.-C.; Yu, D.-P.; Liao, Z.-M. Magnetic Moments in Graphene with Vacancies. *Nanoscale* **2014**, *6*, 8814–8821.

(45) Terrones, H.; Lv, R.; Terrones, M.; Dresselhaus, M. S. The Role of Defects and Doping in 2D Graphene Sheets and 1D Nanoribbons. *Rep. Prog. Phys.* **2012**, *75*, 062501.

(46) Krasheninnikov, A. V.; Lehtinen, P. O.; Foster, A. S.; Pyykkö, P.; Nieminen, R. M. Embedding Transition-Metal Atoms in Graphene: Structure, Bonding, and Magnetism. *Phys. Rev. Lett.* **2009**, *102*, 126807.

(47) Tang, Y.; Yang, Z.; Da, X. Trapping of Metal Atoms in the Defects on Graphene. *J. Chem. Phys.* **2011**, *135*, 224704.

(48) Wong, J.; Yadav, S.; Tam, J.; Singh, C. V. A van der Waals Density Functional Theory Comparison of Metal Decorated Graphene Systems for Hydrogen Adsorption. *J. Appl. Phys.* **2014**, *115*, 224301.

(49) Carrasco, J.; Klimeš, J.; Michaelides, A. The Role of van der Waals Forces in Water Adsorption on Metals. *J. Chem. Phys.* **2013**, *138*, 024708.

(50) Casartelli, M.; Casolo, S.; Tantardini, G. F.; Martinazzo, R. Structure and Stability of Hydrogenated Carbon Atom Vacancies in Graphene. *Carbon* **2014**, *77*, 165–174.

(51) Lombardi, J. R.; Davis, B. Periodic Properties of Force Constants of Small Transition-Metal and Lanthanide Clusters. *Chem. Rev.* **2002**, *102*, 2431–2460.

(52) Johll, H.; Wu, J.; Ong, S. W.; Kang, H. C. Graphene-Adsorbed Fe, Co, and Ni Trimers and Tetramers: Structure, Stability, and Magnetic Moment. *Phys. Rev. B* **2011**, *83*, 205408.

(53) Barone, G.; Duca, D.; Ferrante, F.; La Manna, G. CASSCF/CASPT2 Analysis of the Fragmentation of H_2 on a Pd_4 Cluster. *Int. J. Quant. Chem.* **2010**, *110*, 558–562.

(54) Ramos-Castillo, C. M.; Reveles, J. U.; Zope, R. R.; de Coss, R. Palladium Clusters Supported on Graphene Monovacancies for Hydrogen Storage. *J. Phys. Chem. C* **2015**, *119*, 8402–8409.

(55) Fampiou, I.; Ramasubramaniam, A. Binding of Pt Nanoclusters to Point Defects in

Graphene: Adsorption, Morphology, and Electronic Structure. *J. Phys. Chem. C* **2012**, *116*, 6543–6555.

Table 1: Cohesive energy, E_{coh}, characterizing the homonuclear species, calculated by Eq. 4

	E_{coh}/eV		
	$\mathbf{M}_2$	$\mathbf{M}_3$	$\mathbf{M}_4$
Ni	-1.24	-1.61	-1.89
Pd	-0.74	-1.23	-1.53
Re	-1.51	-1.96	-2.65
Pt	-1.56	-2.08	-2.31

Table 2: Interaction energy of metal atoms with both the pristine C_{48} and the defective C_{47} graphene surfaces, $E^{CP}_{INT}[M/C_{48}]$ and $E_{INT}[M^1/C_{47}]$, and dimer nucleation energy, E^2_{nuc}, on C_{47}, as defined by Eq. 2

Ni	**Pd**	**Re**	**Pt**
[a] $E^{CP}_{INT}[M/C_{48}]/eV$			
−0.60	−0.90	−0.18	−1.12
[b] $E_{INT}[M_1/C_{47}]/eV$			
−6.01	−5.06	−7.35	−6.30
[c] E^2_{nuc}/eV			
Ni	**Pd**	**Re**	**Pt**
−2.02	−1.53	−2.16	−2.14
Pd	**Ni**	**Pt**	**Re**
−1.65	−1.80	−1.28	−2.15

[a] Corrected for the BSSE. [b] Uncorrected for the BSSE. [c] The dimeric species can be individuated, considering that the atom in the table main heading (first table row) is the one approaching the atom already placed on the graphene defect, represented either in the seventh or ninth table rows.

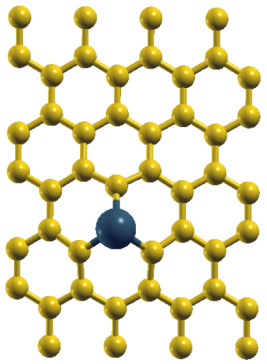

	r(M-C)	g_l
Ni	186	59
Pd	187	63
Re	193	85
Pt	198	72

All values in pm

Figure 1: The M−C bond length in the M^1/C_{47} systems and the values of the buckling parameter, quantifying the graphene distortion following the metal insertion on the defect.

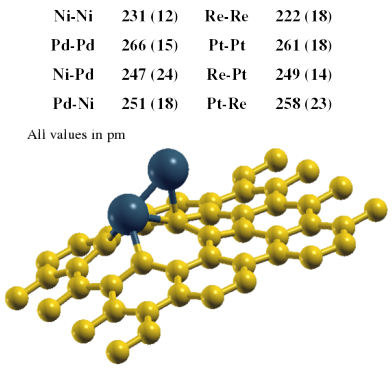

Figure 2: A metallic dimer on a graphene vacancy defect. The M−M bond distances are reported for every homo- and hetero-metallic species along with the differences with respect to the bond lengths calculated for the same species in the isolated states (in parentheses).

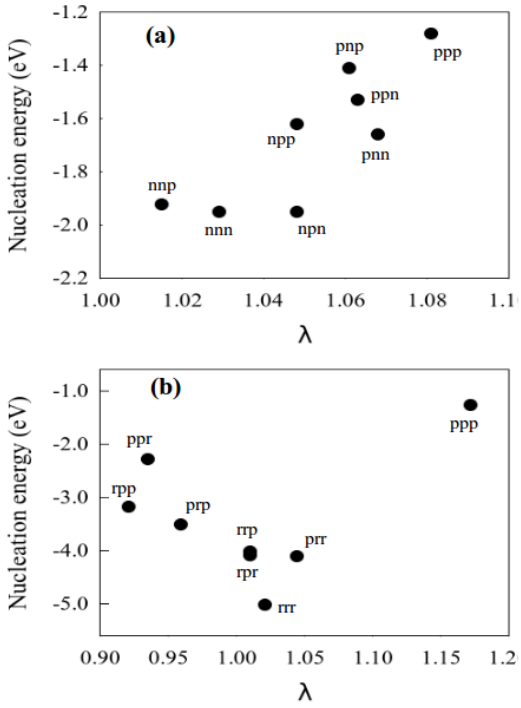

Figure 3: Nucleation energy, E^3_{nuc}, of the homo- and hetero-metallic Ni-Pd (a) and Re-Pt (b) trimers as a function of the bond length distortion parameter, λ. For the sake of clarity, only the initial letter — written in lowercase — of the atomic symbols are represented.

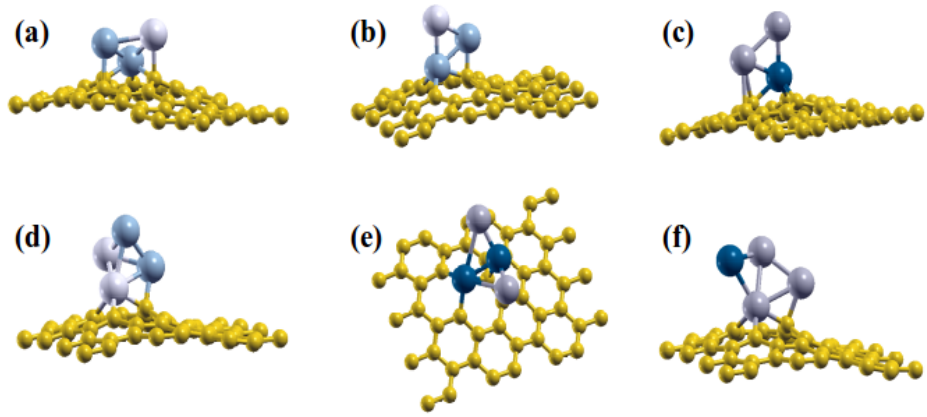

Figure 4: Representative arrangements of three- and four-atom metal clusters on C_{47}. (a) NiPdNi: a triangle lying on the surface; (b) NiNiPd: a triangle in a plane perpendicular to the surface; (c) ReRePt: a different position of the perpendicular triangular geometry; (d) PdNiPdNi: a tetrahedron geometry interacting by a side; (e) ReRePtPt: the butterfly geometry; (f) PtPtPtRe: another arrangement of the butterfly geometry.

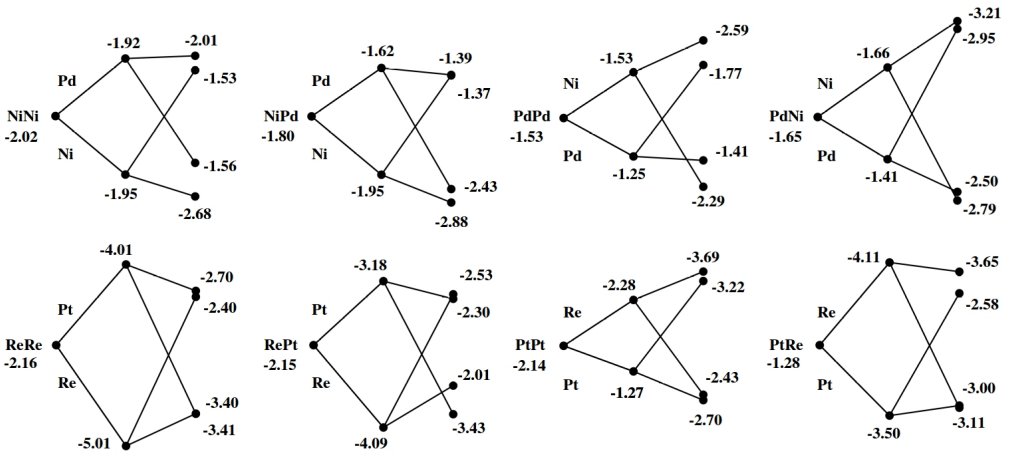

Figure 5: The diagrams collect the nucleation energies (in eV), as defined by Eq. (2), of all the two-atom, E^2_{nuc}, three-atom, E^3_{nuc}, and four-atom, E^4_{nuc}, clusters. In order to assign every point to the corresponding species, start from the two-atom seed and add to it the element symbol indicated above or below it according to whether the given point is in the upper or in the lower part of the diagram with respect to the same seed.

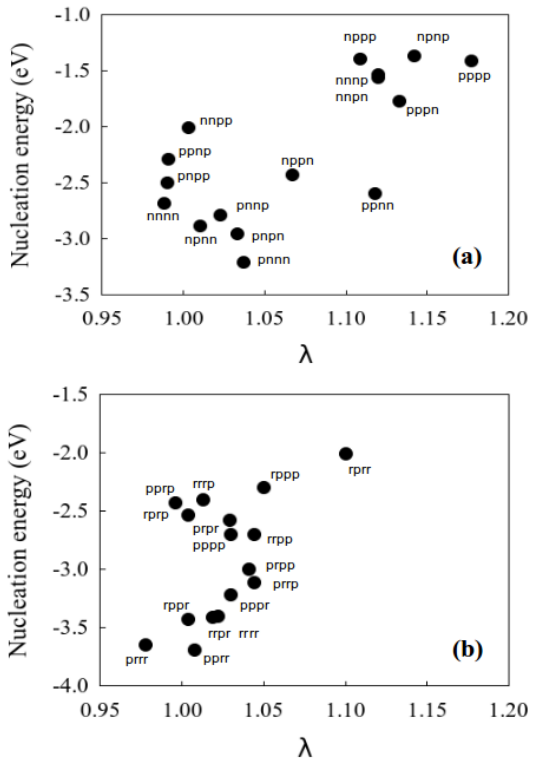

Figure 6: Nucleation energy, E^4_{nuc}, of the homo- and hetero-metallic Ni-Pd (a) and Re-Pt (b) four-atom cluster sets as a function of the bond length distortion parameter, λ. For the sake of clarity, only the initial letter — written in lowercase — of the atomic symbols are represented.